Investigation of operational limit of a pulsating heat pipe by estimating local heat transfer

Naoko Iwata, Fabio Bozzoli (✉)

Department of Engineering and Architecture, University of Parma, Parma 43124, Italy

Abstract

How pulsating heat pipes (PHPs) reach their operational limit has not yet been fully understood. This study aims to provide a complete picture of the termination mechanism of the self-oscillation of vapor and liquid. Experimental studies on a 10-turn PHP with HFC-134a were conducted and the filling ratio (FR) was from 20% to 80%. The thermo-fluid behavior in the PHP was investigated by temperature measurements with a high-resolution and high-speed infrared camera and estimation of fluid-to-wall heat flux distributions by solving inverse heat conduction problems. The results suggested that the PHP, increasing heat load, reached the operational limit due to different mechanisms depending on the filling ratio: at a high FR (80%), the liquid volume ratio increased with the increase of the operating temperature, resulting in the compressed liquid phase. At a low FR (20%), when a large amount of heat was applied, the fluid in the evaporator dried out and became a superheated vapor. The PHP with an optimum FR (50%) transferred the maximum heat under the same evaporator temperature, as the fluid in the PHP was able to keep the saturated two-phase state until the evaporator temperature exceeded the critical temperature.

Keywords

pulsating heat pipe (PHP)
oscillating heat pipe
operational limit
local heat flux
inverse heat conduction problem
infrared measurement

Article History

Received: 27 August 2023
Revised: 8 November 2023
Accepted: 13 November 2023

Research Article

1 Introduction

Recent advances in electronic technology have led to very high-power densities, especially in high-performance chips, with heat fluxes exceeding 30 W/cm^2 at the basic level, and these figures are expected to be even higher in future devices (Agostini et al., 2017). High operating temperatures degrade the reliability and performance of electronic devices, ultimately leading to catastrophic failures. Efficient thermal management is therefore essential to remove heat from heat sources and prevent heat-induced failures. Despite the remarkable advances of the past few decades, thermal management of electronic devices and microprocessors still poses serious technical challenges, one of which is the adequate removal of increased heat flux (Sohel Murshed and Nieto de Castro, 2017). If cooling devices such as fans or cold plates of water loop can be placed adjacent to chips that generate heat, direct cooling is the most straightforward and most efficient in terms of thermal management. Due to the complex layout of dozens of parts in a limited space, it is not always feasible in electric devices including computers. In such cases, a heat transfer device or a heat exchanger, or a chain of them transfers the heat from a chip to the coolant line. In this context, the heat transfer device with high thermal performance such as high thermal conductance is demanded to transfer the heat with minimum temperature difference between the heat source and coolant.

Two-phase heat transfer devices are more efficient than single-phase devices because some or all the heat transport occurs via latent heat. Heat pipes are the classic passive two-phase heat transfer device and are still widely used in electronic devices, ranging from commercial products (Faghri, 2014; Jouhara et al., 2017; Ling et al., 2021) and batteries (Rao et al., 2013) to satellites (Iwata et al., 2018), for decades after their invention (Gaugler, 1944; Grover, 1966). Although heat pipes are very useful, they have a weakness in their wick structure, which is their essential part. The wick structure is inevitable to carry the liquid from a condenser to an evaporator without gravity assistance. Heat pipes should have a wick along the inner wall of the container;

✉ fabio.bozzoli@unipr.it

Nomenclature

C	Thermal conductance (W/K)
C_N	Number of condensers
c_p	Specific heat at constant pressure (J/(kg·K))
d	Diameter (m)
d_{crit}	Critical diameter (m)
G	Overall heat transfer coefficient (W/(m^2·K))
g	Gravity acceleration (m/s^2)
k	Thermal conductivity (W/(m·K))
h_{fg}	Latent heat of vaporization (J/kg)
m_f	Fluid mass (kg)
N	Number of tubes
P	Pressure (Pa)
P_{crit}	Critical pressure (Pa)
P_{exp}	Measured pressure (Pa)
P_{sat}	Saturation pressure (Pa)
Q	Heat (W)
Q_{ele}	Electric power input (W)
Q_{loss}	Heat loss (W)
Q_{net}	Net heat transported by pulsating heat pipe (W)
$Q_{r_{in}}$	Heat from fluid to internal tube wall (W)
$Q_{r_{out}}$	Heat from the tube's external wall to the environment (W)
Q_z	Heat flowing in the axial direction (W)
$Q_{z+\Delta z}$	Heat flowing out in the axial direction (W)
q	Heat flux (W/m^2)
r_{in}	Inner radius (m)
r_{out}	Outer radius (m)
T	Temperature (K)
T_e	Evaporator temperature (K)
T_{env}	Environmental temperature (K)
T_c	Condenser temperature (K)
T_{sat}	Saturation temperature (K)
t	Time (s)
U	Internal energy (J)
V_{PHP}	Internal volume of pulsating heat pipe (m^3)
z	Axial coordinate (m)
β	Liquid volume expansivity (1/K)
γ	Evaporation fraction
κ	Liquid compression factor (1/Pa)
η	Volume ratio of liquid
ρ_l	Liquid density (kg/m^3)
ρ_v	Vapor density (kg/m^3)
ρ_w	Density of tube wall (kg/m^3)
σ	Surface tension (N/m)

this makes them not very easy to be physically flexible, especially for metallic heat pipes. In addition, pressure loss due to the wick affects heat transfer capability; the maximum heat transfer amount limited by the capillary limit decreases as heat pipes get longer.

In the 1990s, a new heat pipe was invented by Akachi (1990, 1993) and Akachi et al. (1996). This heat pipe is called a pulsating heat pipe (PHP) or an oscillating heat pipe because of its operating principle. A PHP consists of a capillary tube or channel repeatedly bent between an evaporator and a condenser. Due to the small hydraulic radius, the working fluid exists as a mixture of liquid slugs and vapor plugs even under gravity. Once heat is applied to the evaporator, self-excited oscillation of the fluid occurs between the evaporator and condenser, which results in heat transfer. One of the favorable features of PHP is that it does not need a wick structure to drive the fluid, unlike other heat pipes. Low-cost, commercially available tubes can be used for PHPs without special processing. This results in an essential advantage for commercial products: the manufacturing cost of the PHP is lower than that of other two-phase thermal devices.

The thermal performance of PHPs is affected by various parameters: geometry, number of turns, tilt angle, inner diameter of tubes/channels, and thermophysical properties of the working fluid. Numerous studies have been conducted, mainly experimentally, to investigate the influence of these parameters. The following is an overview of these studies. Closed-loop PHPs are the preferred structure over open-loop PHPs because they induce circulating flow and higher velocities (Khandekar et al., 2004), provide higher thermal performance, and have been widely studied (Zhang and Faghri, 2008). The number of turns, i.e., the number of bent sections (generally on one side), affects the heat transfer performance of PHP, and increasing the number of turns improves the performance of PHP (Charoensawan et al., 2003) because increasing the number of turns boosts the pressure disturbance and the motion of the working fluid (Quan and Jia, 2009). In addition, Khandekar and Groll (2004) reported that the increment in the number of turns leads to a higher level of perturbations. The number of turns and the orientation or inclination angle of PHP are closely related. Past studies (Iwata et al., 2021) reported that PHPs with a small number of turns, typically less than ten turns, did not operate in horizontal orientation or top heated mode unless they had check valves. In their review article, Han et al. (2016) discussed the existence of the critical number of turns to make the performance of PHP independent of the inclination angle and proposed that increasing the number of turns helps strengthen the

internal pressure fluctuation and weaken the influence of gravity. Several findings have been presented regarding the inner diameter. Many studies have reported that increasing the inner diameter while remaining within the critical diameter improves the heat transfer performance of PHPs (Charoensawan and Terdtoon, 2008; Yang et al., 2008). This is presumably because increasing the inner diameter increases the heat transfer area and decreases the pressure drop. However, there have been several reports that PHPs with smaller diameters have better thermal performance than PHPs with larger diameters (Saha et al., 2012). The thermophysical properties of the working fluid also affect the thermal performance of the PHP. Generally, fluids with the following properties are considered desirable: low viscosity, high partial derivative of temperature with respect to pressure at saturation condition, high thermal conductivity, low latent heat, and high specific heat (Zhang et al., 2008; Taft et al., 2012; Han et al., 2016). To enhance the performance of PHPs, mixtures of two pure fluids (Pachghare and Maballe, 2013) or mixtures of fluids and nanoparticles (Chen and Li, 2020; Zhang et al., 2022) or surfactants (Basatakoti et al., 2020) have been proposed.

So far, a number of PHP's potential applications have been proposed (Zhang and Faghri, 2008; Han et al., 2016). For space applications, PHPs are beginning to be installed on satellites as actual thermal control devices, not for experimental use (AFRL, 2021). However, PHP has not yet been fully practical due to the lack of unified modeling for hydrodynamic and heat transport mechanisms, particularly at the operational limit of PHPs. The operational limit of a PHP is the state where the working fluid inside the PHP does not undergo self-oscillation and the heat transfer from the evaporator to the condenser is drastically reduced. If the heat input to the evaporator continues after the operational limit is reached, the evaporator temperature rises immediately, and the internal pressure of the PHP also increases. In the worst case, this destroys the PHP. In addition, the equipment cooled by the PHP heats up due to the lack of heat transfer, which may cause serious damage to the equipment. Therefore, it is essential to design PHPs so that they do not reach their operational limit during functioning. However, critical PHP features, including the dry-out limit, have not been fully understood yet (Nikolayev, 2021). Mameli et al. (2022) also stated, in the recently published review article on PHP studies, that the major challenge for PHP numerical simulation code is to predict the operational limit.

The amount of heat transfer just before the PHP reaches its operational limit is called the maximum heat transfer rate and has been measured in various studies (Yang et al., 2008; Yin et al., 2016). However, there is no satisfactory model to predict the maximum heat transfer rate because of complicated thermofluidic non-equilibrium phenomena and the large number of complex parameters related to heat transfer in PHPs. Several studies proposed how PHPs reach their operational limit: Yin et al. (2016) assumed the change of flow pattern from slug flow to annular flow causes the limit; Kim and Kim (2020) observed the dry-out phenomenon in a micro-PHP, where all the liquid accumulates in the condenser and is no longer present in the evaporator; Iwata et al. (2016) proposed that liquid occupies the entire PHP due to increasing liquid volume as the operating temperature increases; Drolen and Smoot (2017) proposed six different limits, Bond number limit, vapor inertia limit, heat flux limit, viscous limit, sonic limit, and limitations on heated length and developed analytical tools for prediction. On the other hand, it is not yet clear why several different mechanisms lead PHP to its operational limits and under what conditions these limits are reached. This study aims to provide a more complete picture of the termination mechanism of the self-oscillation of vapor and liquid.

Recently, Iwata et al. (2022) characterized the thermofluid behavior in a micro-PHP by infrared measurement and estimation of fluid-to-wall heat flux distributions by solving inverse heat conduction problems. In this study, the authors investigate the operational limit of the PHP by extending the methods and conducting experiments on a 10-turn PHP with HFC-134a (1,1,1,2-tetrafluoroethane) at a filling ratio of 20%–80%. The final goal is to explain the behaviors of fluid up to the operational limits and how this can vary with the filling ratio, providing a complete picture of the termination mechanism of the self-oscillation of vapor and liquid.

2 Experimental setup

A stainless-steel tube with inner and outer diameters of 0.88 and 1.59 mm, respectively, was bent into 10 turns as sketched in Fig. 1. For the working fluid of HFC-134a, in the temperature range from 7 °C (280 K) to 77 °C (350 K), the inner diameter is less than the critical maximum diameter d_{crit} defined by Eq. (1) (Ma, 2015):

$$d_{\mathrm{crit}} = 2\left[\frac{\sigma}{g\left(\rho_{\mathrm{l}} - \rho_{\mathrm{v}}\right)}\right]^{1/2} \tag{1}$$

where σ, g, ρ_{l}, and ρ_{v} are the surface tension, gravitational acceleration (9.81 m/s^2), liquid density, and vapor density, respectively. Using the properties of NIST Reference Fluid Thermodynamic and Transport Properties Database mini-REFPROP version 10.0 (National Institute of Standards and Technology, 2013), d_{crit} at 7 and 77 °C are calculated to

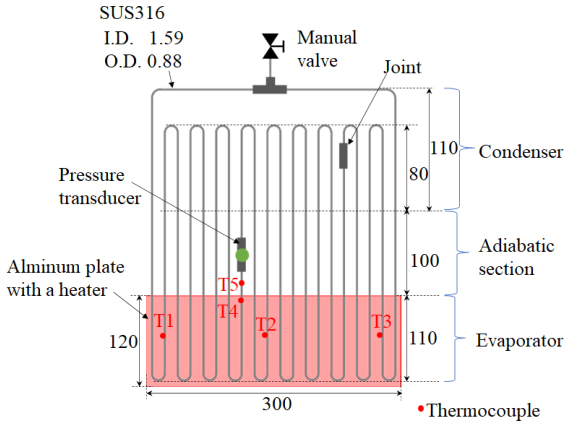

Fig. 1 Schematic of PHP (unit: mm).

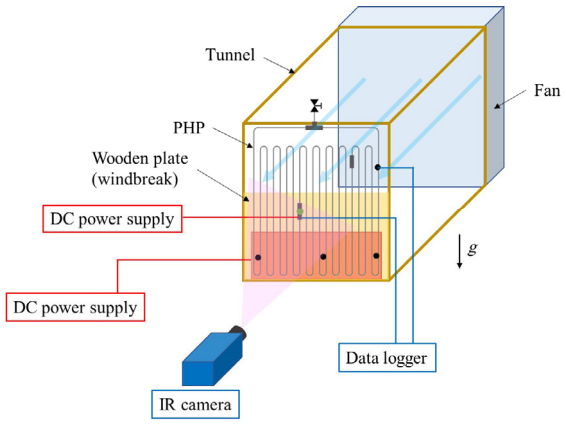

Fig. 2 Experimental setup.

be 1.8 and 0.99 mm, respectively. The tubes in the evaporator were attached to a 1.5-mm-thick aluminum spreader by aluminum tapes, while the heat load was provided by a silicone-rubber sheet heater (OMEGA SRFGA-412/10), placed on the back of the spreader.

For charging, first the PHP and the tubes connected to it were vacuumed to below 30 Pa by a vacuum pump (AGILENT DS40M). The pressure was measured by a vacuum gauge (AGILENT 0531TC) and a controller (AGILENT RGC-150). Then HFC-134a (C2H2F4, purity ≥ 98.5%) was used as a working fluid. The filling ratio was changed to 20%, 30%, 50%, 70%, and 80%. The filling ratio was defined as the ratio of the liquid working fluid volume to the total PHP volume at 20 °C and was checked by measuring the weight of the PHP with and without the fluid on a precision electronic balance (KERN EG620-3NM) which has a readability of 0.001 g and a verification value of 0.01 g. A fluid mass of 0.01 g corresponds to 0.7% of the fluid mass in the loop at a 100% filling ratio at 20 °C.

The PHP was placed at the outlet of a wind tunnel to cool the upper section (i.e., condenser) as shown in Fig. 2. A shield between the tunnel outlet and the PHP prevented the air from flowing on the evaporator and the adiabatic section. Atmospheric air impinged on the PHP at the flow velocity of 3.6 m/s near the condenser. The condenser temperature was monitored by an infrared camera (FLIR SC7000, space resolution: 640 pixels × 512 pixels, accuracy: ±1 K, thermal sensitivity at 303 K: 20 mK). The tubes in the condenser and adiabatic sections were coated with a thin film of water-soluble, high-emissivity paint. The effective emissivity of the coating was estimated in situ by shooting the target at various known temperatures, yielding a value of 0.95±0.01 (Cattani et al., 2022). To manage the correspondence between the measurements made by the two measurement systems, the temperature at one point was also checked using thermocouples. In order to eliminate the influence of curvature in the infrared measurement, the outer diameter of the tube was taken over three pixels, of which only the single pixel with the highest temperature in the center was considered for evaluation. The temperatures of the evaporator and adiabatic section were measured with T-type thermocouples at five locations, as shown in Fig. 1. A pressure transducer (Kulite XTEL-190S-1000A) was mounted in the tube of the adiabatic section. During the tests, the PHP operated in vertical bottom heat mode, i.e., with the evaporator at the bottom. A stepwise heat load was provided to the evaporator from 47 W by a DC power supply (Aim-TTi CPX400D) until the PHP reached the operational limit, i.e., the evaporator temperature rose rapidly, or the evaporator temperatures exceeded the critical temperature of HFC-134a, 101 °C. The experimental data were collected by a data acquisition system (AGILENT 34970A), for each power input, when the device reached the pseudo-steady state or the operational limit.

3 Heat flux estimation

Using the time-space temperature maps acquired by the infrared camera as input data, the local wall-to-fluid heat flux was evaluated by solving the inverse heat conduction problem at the tube wall. Specifically, each straight part of the PHP channels belonging to the condenser section was modeled as a 2D-axisymmetric solid domain, outlined in Fig. 3. By assuming the thin-wall approximation, the temperature on the external surface was considered equal to that on the internal surface. In addition, due to experimental

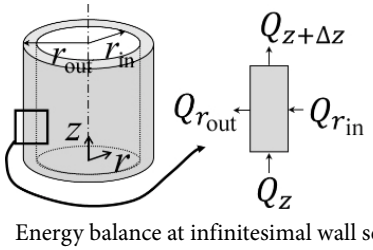

Fig. 3 Energy balance at infinitesimal wall section.

observations, the temperature gradients along the tube circumference were considered to be negligible.

Following the previous assumptions, the energy balance equation becomes

$$\frac{\mathrm{d}U}{\mathrm{d}t} = Q_z - Q_{z+\Delta z} + Q_{r_{\mathrm{in}}} - Q_{r_{\mathrm{out}}} \tag{2}$$

where Q_z and $Q_{z+\Delta z}$ are the conductive terms related to the axial direction z, while $Q_{r_{\mathrm{out}}}$ is the power dissipated to the environment by natural convection. The time derivative of internal energy $\mathrm{d}U/\mathrm{d}t$ is expressed as

$$\frac{\mathrm{d}U}{\mathrm{d}t} = \rho_{\mathrm{w}} c_p \frac{\partial T}{\partial t} \cdot \pi(r_2^2 - r_{\mathrm{in}}^2) \cdot \Delta z \tag{3}$$

where ρ_{w} and c_p are the stainless-steel density and specific heat, respectively. By expressing the power terms of Eq. (2), and combining Eqs. (2) and (3), the heat flux q, exchanged between the working fluid and the inner wall of the channel, can be finally expressed as

$$q = \frac{\left(\rho_{\mathrm{w}} c_p \frac{\partial T}{\partial t} - k\frac{\partial T^2}{\partial z^2}\right) \cdot ({r_{\mathrm{out}}}^2 - {r_{\mathrm{in}}}^2) + \frac{T - T_{\mathrm{env}}}{G} \cdot 2r_{\mathrm{out}}}{2r_{\mathrm{in}}} \tag{4}$$

where r_{out}, r_{in}, T_{env}, and G are the outer radius of the tube, the inner radius of the tube, the ambient temperature, and the overall heat-transfer coefficient between the channel wall and the surrounding environment, respectively.

The environment temperature measured during the experiment was assigned to T_{env} in Eq. (4). Due to the noise level of the infrared raw data (Rainieri et al., 2008), a regularization method was applied to the temperature distributions to reliably solve it. The processing target area of the condenser is every straight tube where the distance from the U-shaped apex is from 12 to 76 mm, which is equivalent to 160 pixels in the longitudinal direction of the IR camera as shown in Fig. 4.

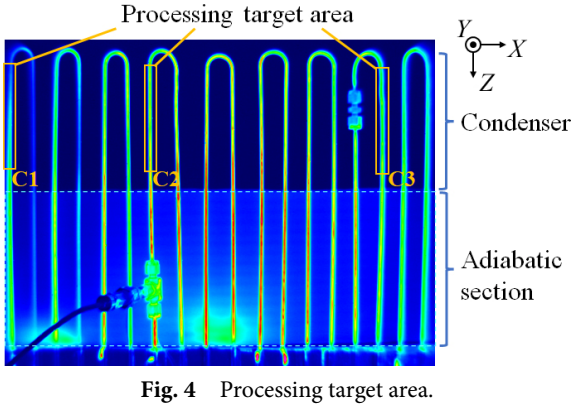

Fig. 4 Processing target area.

4 Results and discussion

4.1 Heat transfer performance

The thermal conductance C was evaluated as the thermal performance of the PHP. It is obtained from Eq. (5):

$$C = \frac{Q_{\mathrm{net}}}{T_{\mathrm{e}} - T_{\mathrm{c}}} \tag{5}$$

where T_{e} and T_{c} are the evaporator and condenser temperatures, respectively. The evaporator temperature was evaluated by averaging the temperatures measured with thermocouples for 120 s in a pseudo-steady state, as expressed by Eq. (6):

$$T_{\mathrm{e}} = \frac{\mathrm{T1} + \mathrm{T2} + \mathrm{T3}}{3} \tag{6}$$

where T1, T2, and T3 correspond to the thermocouples shown in Fig. 1. The condenser temperature was derived from averaging the temperatures of 160 pixels in the areas indicated by C1, C2, and C3 in Fig. 4. Since these areas included other than tube surfaces, the maximum temperature was extracted from the transverse temperatures at each Z-directional position and used as the condenser surface temperature. In Eq. (5), Q_{net} indicates the net heat input to the evaporator, which is calculated by Eq. (7):

$$Q_{\mathrm{net}} = Q_{\mathrm{ele}} - Q_{\mathrm{loss}} \tag{7}$$

where Q_{ele} and Q_{loss} are the electrical power input and the heat loss from parts other than the condenser to the ambient air, respectively. The heat leak was calculated from the averaged surface temperature and surface area of the evaporator or adiabatic section, the averaged ambient air temperature, and the convective heat transfer coefficient obtained by a preliminary test with a sample tube.

The measurement uncertainties of the T-type thermocouple and the voltage and the current of the power supply were ±0.2 °C, ±(0.1% of reading value + 2 digits), and ±(0.3% of reading value + 2 digits), respectively. The measurement uncertainty of the data acquisition system for the temperature measurement was 1.0 °C. The overall uncertainty of the thermal conductance was estimated based on the error propagation methods described by Moffat (1988) and was found to be less than 4% for all the input power levels.

Figure 5 shows the correlation between the thermal conductance of the PHP at each filling ratio and the net heat input. The conductance was more than 0.25 K/W apart from the PHP with FR 20%. The conductance of the PHP with FR 70%, 50%, and 30% decreased when the maximum heat load was applied or even several watts before that. On

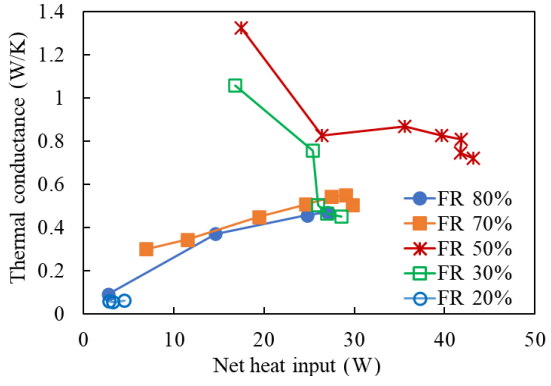

Fig. 5 Correlation between net heat input and thermal conductance.

the other hand, the conductance at FR 80% monotonically increased with the increase of the heat input. The conductance at FR 20% was less than one-fifth that of the other PHPs. Pure thermal conduction, i.e., the thermal conductance of the empty PHP was calculated to be 0.00441 W/K and verified by the experiment, which meant that the FR 20% PHP was also operating as a PHP or a thermosyphon. The PHP with FR 50% showed the best performance in terms of the conductance and the maximum heat load, as reported by the previous studies (Han et al., 2016).

The thermal conductance against the evaporator temperature T_e is plotted in Fig. 6. All the PHP was tested until the evaporator temperature exceeded the critical temperature as none of them showed a rapid increase in the evaporator temperature during the test. This was why the maximum evaporator temperature for each FR was in the range of 105–115 °C. Comparing Fig. 5 and Fig. 6, it can be said that the correlation between the conductance and the heat input strongly varied with the FR, while the correlation between the conductance and the evaporator temperature, except for the PHP with FR 20%, showed a weak variation with the FR. These observations suggest that the PHP reached the operational limit through different

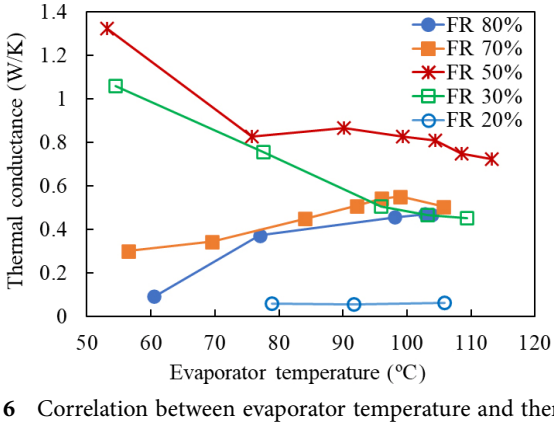

Fig. 6 Correlation between evaporator temperature and thermal conductance.

mechanisms depending on the FR, which will be discussed in Sections 4.2, 4.3, and 4.4.

4.2 Operational limit of PHP with a high filling ratio

Figure 7 shows the histories of the temperatures (T_e and T5 shown in Fig. 1), pressure, and power input of the PHP with FR 80%. The measured pressure and critical pressure of HFC-134a are expressed as P_{exp} and P_{crit}, respectively, in the legend of Fig. 7. At the power input of 98 W, the pressure increased to 4.8 MPa exceeding the critical pressure of 4.059 MPa. On the other hand, the temperatures of both the evaporator and the adiabatic section were still lower than the critical temperature of 101 °C. Moreover, when the power input was increased to 105 W, the temperatures increased only 2–3 °C, while the pressure increased by 1 MPa. Considering the derivative of pressure with respect to the temperature at the saturation state (dP/dT_{sat}) of HFC-134a is less than 0.075 MPa/K, the fluid state in the PHP was not the saturated two-phase state but it was either supercritical fluid or compressed liquid as shown in the phase diagram in Fig. 8.

Figure 9 shows a representative IR image of the condenser and adiabatic section of the PHP with FR 80% at the power input of 105 W, which was the maximum power input kept to the steady state. The temperature distribution

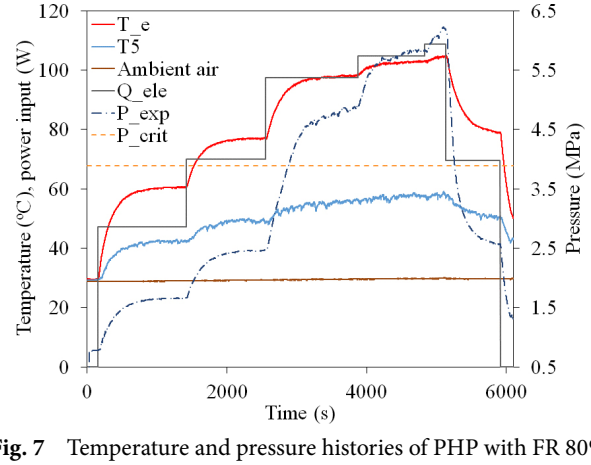

Fig. 7 Temperature and pressure histories of PHP with FR 80%.

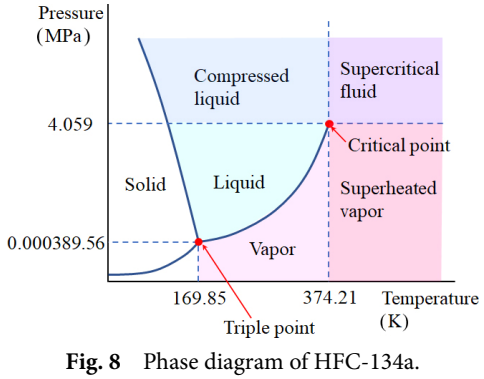

Fig. 8 Phase diagram of HFC-134a.

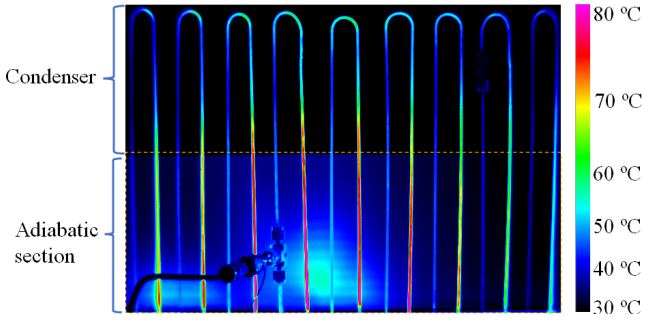

Fig. 9 Infrared image of the condenser and adiabatic section of PHP with FR 80% at Q_{ele} = 105 W.

of the right-hand tube with temperatures falling from bottom to top and from top to bottom in the left-hand tube, suggested the existence of a unidirectional flow from the right to left in every tube with one U-shaped bend. The condenser temperature was distributed from 30 to 70 °C, while that of the adiabatic section was 40 to 85 °C. The fluid coming from the evaporator flowed through the adiabatic section and was cooled in the condenser, and then went down to the evaporator through the adiabatic tube on the other side.

Figure 10 shows the filtered temperature and heat flux of area C2 (i.e., a portion of the condenser) in Fig. 4 of the PHP with FR 80%. The IR images taken at a one-minute steady state at the heat input of 105 W were processed. The fluctuations in heat flux suggested the active oscillation of the fluid, even though it was not easily noticeable by the temperature maps. The heat flux varied from 600 W/m^2 to 10,600 W/m^2, mainly depending on the location. This suggested the presence of a steady liquid lump with relatively low temperature and thus low heat exchange with ambient air, in the middle of the condenser tube. As previously mentioned, the fluid was supposed not to be in the saturated two-phase state in the PHP with FR 80% at the power input of more than 105 W. The flow pattern was therefore not a slug/plug flow, but natural convection alone, with the fluid circulating. Considering the low temperature

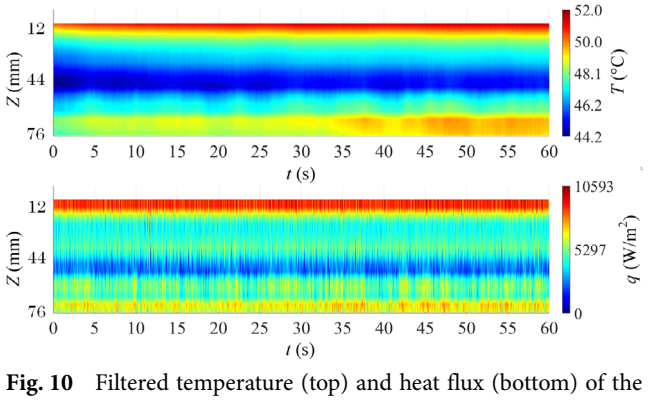

Fig. 10 Filtered temperature (top) and heat flux (bottom) of the condenser of PHP with FR 80% at Q_{ele} = 105 W.

in the condenser and the adiabatic section, the fluid was estimated to be a compressed liquid rather than a supercritical fluid.

In terms of pressure changes, this also suggested that the fluid was a single-phase compressed liquid. The pressure change of a liquid was expressed as Eq. (8):

$$dP = \frac{\beta}{\kappa} dT \tag{8}$$

where β and κ are the liquid volume expansivity and liquid compression factor, respectively. Assuming β and κ in HFC-134a liquid at 97 °C are 0.055237 K^{-1} and 0.16701 MPa^{-1} (National Institute of Standards and Technology, 2013), 1 °C temperature rise in the fluid results in a 0.33 MPa pressure increase. This agreed with the temperature and pressure histories at the heat input of 105 W.

The reason for the transition of the two-phase fluid to liquid can be explained by the increase in the ratio of the liquid in the PHP to the total volume of the PHP as the operating temperature increases. The liquid density increases and vapor density decreases with the increase of the saturation temperature. Assuming the working fluid in the PHP is in a two-phase fluid at a certain saturation temperature T_{sat}, the volume ratio of the liquid η is expressed as Eq. (9):

$$\eta = \frac{m_f - \rho_v \cdot V_{PHP}}{(\rho_v - \rho_l) V_{PHP}} \tag{9}$$

where m_f, V_{PHP}, ρ_l, and ρ_v are the fluid mass, the internal volume of the PHP, liquid density, and the vapor density at T_{sat}, respectively. Substituting the estimated value of 4.26 cm^3 for V_{PHP} and measured value of 4.20 g for m_f, η for the PHP with FR 80% concerning T_{sat} was as shown in Fig. 11. The densities, ρ_l and ρ_v, were derived from mini-REFPROP (National Institute of Standards and Technology, 2013). From Fig. 11, it can be seen that η increased as T_{sat} rose, and eventually, the PHP was fully occupied by the single-phase liquid at T_{sat} of 72 °C, which was close to the arithmetic mean of the evaporator and condenser temperatures at steady state at Q_{ele} of 105 W, i.e., 74 °C. Assuming that the fluid was in the saturation two-phase state at a uniform operating temperature which corresponded to the arithmetic mean of the evaporator and condenser temperatures, the above result also suggested that the PHP could reach the operational limit because of the phase change from the two-phase to the single liquid phase. Thanks to the effects of natural convection and inertia of the fluid motion in slug/plug flow, the thermal conductance did not drop radically even after the liquid occupied the whole PHP.

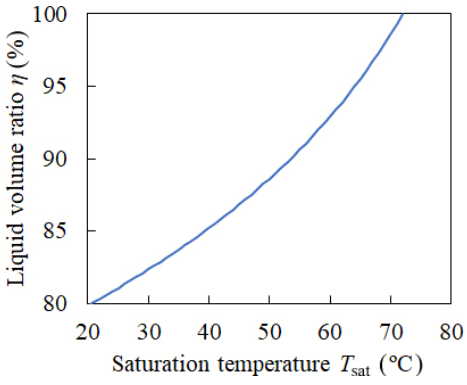

Fig. 11 Liquid volume ratio of PHP with FR 80% with respect to saturation temperature.

4.3 Operational limit of PHP with a low filling ratio

Figure 12 shows the histories of the temperature, pressure, and power input of the PHP with FR 20%. Immediately after the heat was applied to the evaporator, the pressure and condenser temperature rose rapidly, which indicated the start-up of the PHP. Then, however, they did not increase as high as those of the PHP with FR 80%, though the pressure fluctuated indicating the fluid oscillation. The evaporator temperature increased up to 106 °C at the power input of 70 W, exceeding the critical temperature of HFC-134a, but the average pressure remained at 0.91 MPa, which corresponded to the saturation temperature of 35 °C. This indicated that the PHP reached the operational limit through a different flow regime from the PHP with FR 80%.

A representative IR image of the condenser and adiabatic section of the PHP with FR 20% at the power input of 70 W is shown in Fig. 13. In the adiabatic section, only the right-side tube of each turn had a high temperature of up to 50 °C, while the others were as low as 32–34 °C, the same temperature as the condenser tubes. This suggested that the

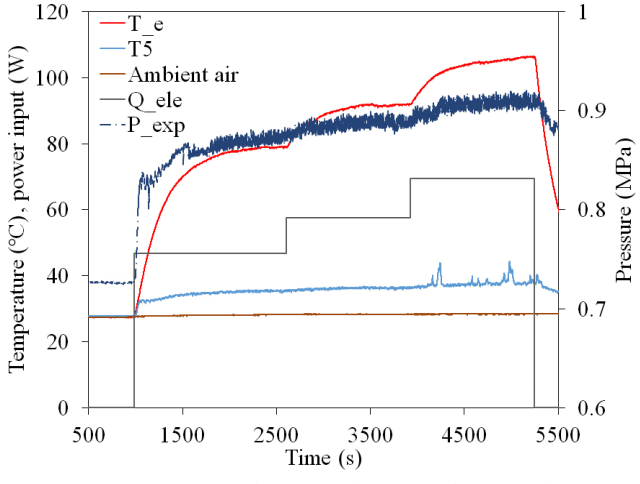

Fig. 12 Temperature and pressure histories of PHP with FR 20%.

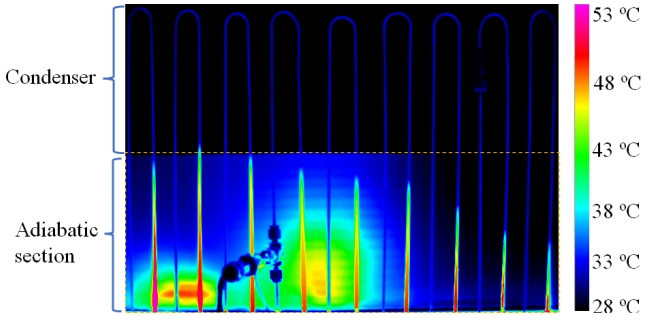

Fig. 13 Infrared image of the condenser and adiabatic section of PHP with FR 20% at Q_{ele} = 70 W.

fluid existed in the PHP in different states depending on the positions. In the evaporator, superheated vapor shown in Fig. 8 existed as its temperature exceeded the critical temperature while its pressure was below the critical pressure. The superheated vapor rose toward the condenser and was gradually cooled by the heat exchange with the ambient air. When the vapor was cooled sufficiently in the middle of the adiabatic section or the condenser, the superheated vapor turned to the two-phase flow. More vapor started condensing in the condenser and flew down to the evaporator through the other side of the tube, i.e., the left-side tube of each turn, which had a lower temperature than the right-side tubes in Fig. 13.

A question then arose: "What is the flow regime in the condenser?" Considering the heat exchange with the environment, condensation occurred on the inner wall of the tube. Assuming that the inner walls of all condenser tubes and half of the adiabatic section tube were wetted with a thin liquid film of 100 μm in thickness, the liquid mass was calculated to be 1.00 g. This corresponded to 96% of the total fluid mass in the PHP with FR 20%. This suggested that liquid slugs hardly existed in the condenser and the flow regime was unlikely slug/plug flow. This could be explained by another aspect: the driving force was presumably not sufficient to induce and maintain the fluid oscillation.

Figure 14 shows the filtered temperature and heat flux of area C2 in Fig. 4 of the PHP with FR 20%. The IR images taken at a one-minute steady state at the heat input of 70 W were processed. The temporal and spatial distribution of the temperature was only 1 °C. Furthermore, the heat flux also only varied from 400 to 1200 W/m^2, though fluctuation was observed. This suggested the thin film condensation on the wall and flowing down to the evaporator by gravity, rather than an oscillating slug/plug flow. In summary, when the FR was small and the amount of the fluid was not enough to keep the oscillating slug/plug flow, eventually the fluid in the evaporator became superheated vapor. In this experiment, the PHP was placed in the bottom heated

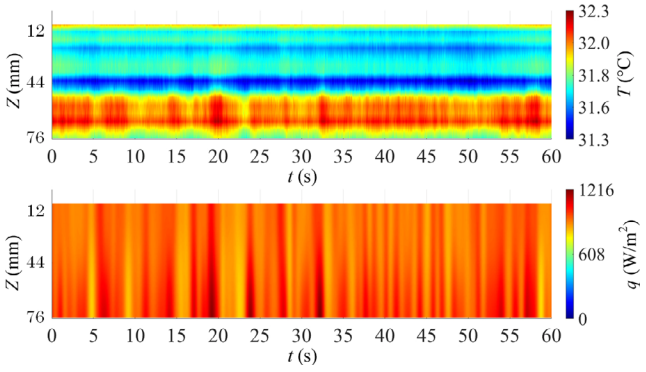

Fig. 14 Filtered temperature (top) and heat flux (bottom) of the condenser of PHP with FR 20% at Q_{ele} = 70 W.

orientation, and hence, even in this situation, the PHP did not completely lose its heat transfer function and acted as a kind of thermosyphon.

4.4 Operational limit of PHP with an optimum filling ratio

Figure 15 shows the histories of the temperature, pressure, and power input of the PHP with FR 50%, the optimum FR for this PHP. The temperatures of the evaporator and condenser and the pressure increased with the increase of the power input. Even after the evaporator temperature reached and exceeded the critical temperature of HFC-134a, the pressure remained below the critical pressure and increased at a rate of increase with respect to temperature (dP/dT) around 0.02 MPa/K. It was therefore unlikely that the fluid was in the compressed liquid phase.

Figure 16 shows a representative IR image of the condenser and adiabatic section of the PHP with FR 50% at the power input of 167 W, the maximum power input for this PHP. Unlike the two previous results of the high and low FRs, the temperature of left-sided tubes was higher than the right-sided tube in each turn, indicating that the fluid circulated from left to right. Furthermore, the condenser

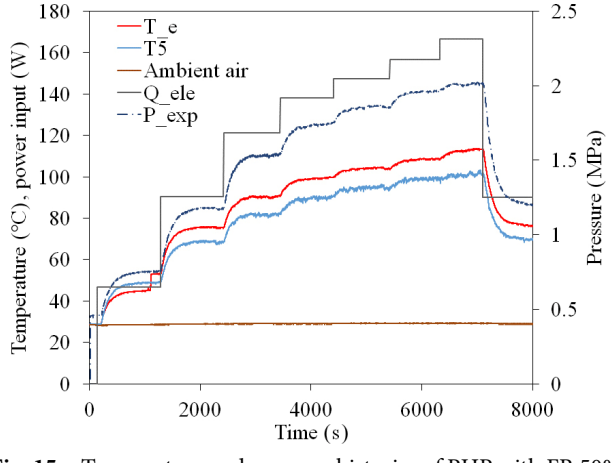

Fig. 15 Temperature and pressure histories of PHP with FR 50%.

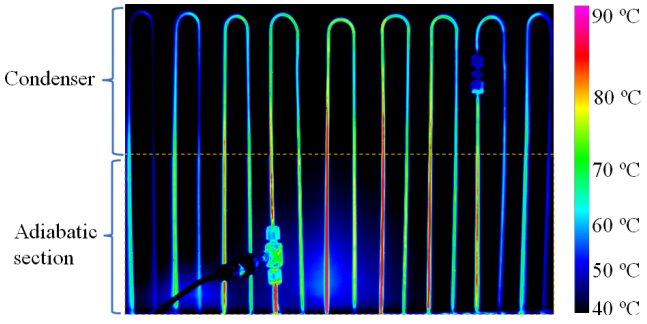

Fig. 16 Infrared image of the condenser and adiabatic section of PHP with FR 50% at Q_{ele} = 167 W.

temperature was as high as 45–85 °C. From the measured temperature and the pressure, the fluid in the adiabatic section was estimated to be in a two-phase state, close to the critical point in the left tube and around 45–80 °C in the right tube. There were two possibilities for the fluid state in the evaporator, given that its temperature was above the critical temperature: if the fluid pressure in the evaporator was above the critical pressure, the fluid was supercritical; otherwise, it was superheated vapor. Since the evaporator pressure was not directly measured, it could not be stated.

Figure 17 shows the filtered temperature and heat flux of area C2 in Fig. 4 of the PHP with FR 50%. The IR images taken at a one-minute steady state at the heat input of 167 W were processed. The heat flux varied from 10,000 to 16,000 W/m² with the fluctuation. This suggested oscillation or circulation of a two-phase flow, presumably a slug/plug flow or annular flow, but further investigation is required to determine which it was.

Regarding the operational limit caused by change of the flow pattern, Drolen and Smoot (2017) proposed an equation to predict a vapor inertia limit that the liquid meniscus of the advancing slug can withstand without being forced to transition into annulus. For the laminar flow, the equation based on the maximum vapor inertia forces is derived as Eq. (10):

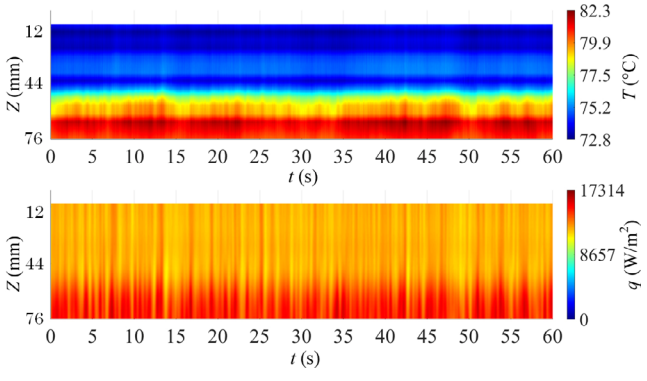

Fig. 17 Filtered temperature (top) and heat flux (bottom) of the condenser of PHP with FR 50% at Q_{ele} = 167 W.

$$Q = \frac{1.924 N C_N r_{out} h_{fg}}{\gamma} \sqrt{\sigma \rho_v r_{out} (\cos\theta_r - \cos\theta_a)} \qquad (10)$$

where N, C_N, h_{fg}, γ, θ_a, and θ_r are the number of tubes, number of condensers, latent heat of vaporization, evaporation fraction, advancing contact angle, and receding contact angle, respectively. Assuming γ, θ_a, and θ_r to be 0.5, 7 deg (Vadgama and Harris, 2007; Lu et al., 2016), and 0 (Drolen and Smoot, 2017) respectively, we obtained Fig. 18 for the present PHP. The thermophysical properties are derived from mini-REFPROP version 10.0 (National Institute of Standards and Technology, 2013).

Figure 18 suggests the flow in the PHP at the maximum heat input already transited to the annular flow since the net heat input was 43 W. The fluid in the PHP was able to circulate between the evaporator and the condenser by the gravity effect, even after the transition to the annular flow.

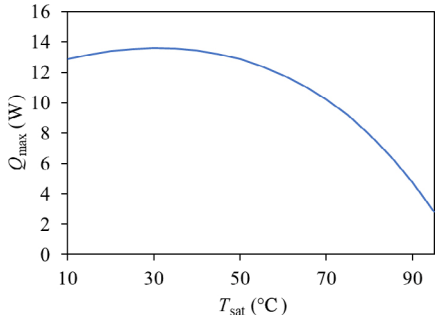

Fig. 18 Vapor inertia transport limit.

5 Conclusions

Although PHP is a promising heat transfer device and a number of its potential applications have been proposed, PHP has not yet been fully practical due to the lack of unified modeling for hydrodynamic and heat transport mechanisms, particularly at the operational limit of PHPs. This study aims to provide a more complete picture of the termination mechanism of the self-oscillation of vapor and liquid in a PHP. Experimental studies on a 10-turn PHP with HFC-134a were conducted by changing the filling ratio from 20% to 80%. The thermo-fluid behavior in the PHP at the operational limit and transition to it was investigated by temperature distribution measurements with a high-resolution and high-speed infrared camera and estimation of fluid-to-wall heat flux distributions by solving inverse heat conduction problems. The outcomes are as follows:

1) The results suggested that the PHP reached the operational limit in the different mechanisms depending on the filling ratio.
2) At a high FR (80%), the liquid volume ratio increased with the increase of the operating temperature, resulting in the compressed liquid phase, which suppressed the fluid oscillation. This was supported by the experimental results: a) the pressure of the inner PHP exceeded the critical pressure of HFC-134a, while the evaporator temperature was still below the critical temperature; b) the measured pressure changes with respect to the temperature agreed with that of the compressed liquid; c) the measured temperature at which the pressure reached the critical pressure agreed with the predicted one at which the liquid volume ratio reached 100%. The heat flux at the condenser and adiabatic section varied from 600 W/m^2 to 10,600 W/m^2, mainly depending on the location.
3) At the low FR (20%), when a large amount of heat was applied, the fluid in the evaporator dried out and became a superheated vapor. This was supported by the fact that the evaporator temperature exceeded the critical temperature even though the measured pressure was less than a quarter of the critical pressure. Moreover, the heat flux was ranged only from 400 to 1200 W/m^2. The PHP was placed in bottom heated mode and thus operated as a thermosyphon after it reached the operational limit: the vapor cooled in the condenser condensed on the inner walls and returned to the evaporator.
4) The PHP with the optimum FR (50%) transferred the maximum heat under the same evaporator temperature, as the fluid in the PHP was able to keep the saturated two-phase state until the evaporator temperature exceeded the critical temperature. The heat flux varied from 10,000 to 16,000 W/m^2 with the fluctuation. There were two possibilities for the fluid state in the evaporator: if the fluid pressure in the evaporator was above the critical pressure, the fluid was supercritical, otherwise, it was superheated vapor. Since the evaporator pressure was not measured, it could not be determined.

Further investigations, such as evaporator pressure measurements and visualization tests, are needed to fully understand the mechanisms of the operational limits of PHPs with an optimum FR. Furthermore, it should be noted that the operational limits of PHPs are supposed to be influenced by the cooling method and there might be other mechanisms by which a PHP cooled by a more powerful cooling method, such as water cooling, reaches its limits.

Funding note

Open access funding provided by Università degli Studi di Parma within the CRUI-CARE Agreement.

Acknowledgements

This work has received funding from the European Union's Horizon 2020 research and innovation programme under the Marie Skłodowska-Curie (Grant No. 894750).

Declaration of competing interest

The authors have no competing interests to declare that are relevant to the content of this article.

References

Agostini, B., Torresin, D., Koivuluoma, T., Wang, Y. X. 2017. Self-contained thermosyphon heat exchanger for power converters. *ABB Review*, 4: 14–21.

Air Force Research Laboratory Public Affairs (AFRL). 2021. AFRL, industry launch revolutionary spacecraft technology - Oscillating Heat Pipes. *AFRL News*. Available at https://www.afrl.af.mil/News/Article/2817283/afrl-industry-launch-revolutionary-spacecraft-technology-oscillating-heat-pipes/

Akachi, H. 1990. Structure of a heat pipe. U.S. Patent No. 4,921,041. Washington, DC, USA: U.S. Patent and Trademark Office.

Akachi, H. 1993. Structure of micro-heat pipe. U.S. Patent No. 5,219,020. Washington, DC, USA: U.S. Patent and Trademark Office.

Akachi, H., Polasek, F., Stluc, P. 1996. Pulsating heat pipes. In: Proceedings of the 5th International Heat Pipe Symposium, Melbourne, Australia: 208–217.

Basatakoti, D., Zhang, H., Li, X., Cai, W., Li F. 2020. Visualization of bubble mechanism of pulsating heat pipe with conventional working fluids and surfactant solution. *Experimental and Computational Multiphase Flow*, 2: 22–30.

Cattani, L., Mangini D., Bozzoli, F., Pietrasanta, L., Mameli, M., Filippeschi, S., Rainieri, S., Marengo, M. 2019. An original look into pulsating heat pipes: Inverse heat conduction approach for assessing the thermal behaviour. *Thermal Science and Engineering Progress*, 10: 317–326.

Cattani, L., Vocale, P., Bozzoli, F., Malavasi, M., Pagliarini, L., Iwata, N. 2022. Global and local performances of a tubular micro-pulsating heat pipe: Experimental investigation. *Heat and Mass Transfer*, 58: 2009–2027.

Charoensawan, P., Khandekar, S., Groll, M., Terdtoon, P. 2003. Closed loop pulsating heat pipes Part A: parametric experimental investigations. *Applied Thermal Engineering*, 23: 2009–2020.

Charoensawan, P., Terdtoon, P. 2008. Thermal performance of horizontal closed-loop oscillating heat pipes. *Applied Thermal Engineering*, 28: 460–466.

Chen, M., Li, J. 2020. Nanofluid-based pulsating heat pipe for thermal management of lithium-ion batteries for electric vehicles. *Journal of Energy Storage*, 32: 101715.

Drolen, B. L., Smoot, C. D. 2017. Performance limits of oscillating heat pipes: Theory and validation. *Journal of Thermophysics and Heat Transfer*, 31: 920–936.

Faghri, A. 2014. Heat pipes: Review, opportunities and challenges. *Frontiers in Heat Pipes*, 5: 1.

Gaugler, R. S. 1944. Heat transfer devices. U.S. Patent No. 2,350,348. Washington, DC, USA: U.S. Patent and Trademark Office.

Grover, G. M. 1966. Evaporation-condensation heat transfer device. U.S. Patent No. 3,229,759. Washington, DC, USA: U.S. Patent and Trademark Office.

Han, H., Cui, X., Zhu, Y., Xu, T., Sui, Y., Sun, S. 2016. Experimental study on a closed-loop pulsating heat pipe (CLPHP) charged with water-based binary zeotropes and the corresponding pure fluids. *Energy*, 109: 724–736.

Han, X., Wang, X., Zheng, H., Xu, X., Chen, G. 2016. Review of the development of pulsating heat pipe for heat dissipation. *Renewable and Sustainable Energy Reviews*, 59: 692–709.

Iwata, N., Bozzoli, F., Pagliarini, L., Cattani, L., Vocale, P., Malavasi, M., Rainieri, S. 2022. Characterization of thermal behavior of a micro pulsating heat pipe by local heat transfer investigation. *International Journal of Heat and Mass Transfer*. 196: 123203.

Iwata, N., Miyazaki, Y., Yasuda, S., Ogawa, H. 2021. Thermal performance and flexibility evaluation of metallic micro oscillating heat pipe for thermal strap. *Applied Thermal Engineering*, 197: 117342.

Iwata, N., Ogawa, H., Miyazaki, Y. 2016. Maximum heat transfer and operating temperature of oscillating heat pipe. *Journal of Heat Transfer*, 138: 122002.

Iwata, N., Usui, T., Ikeda, M., Takei, Y., Okamoto, A., Ogawa, H., Yumoto, T., Ono, Y., Kokubun, M., Takahashi, T. 2018. Evaluation of in-orbit thermal performance of X-ray astronomy satellite "Hitomi". *Journal of Spacecraft and Rockets*, 55: 77–84.

Jouhara, H., Chauhan, A., Nannou, T., Almahmoud, S., Delpech, B., Wrobel, L. C. 2017. Heat pipe based systems - Advances and applications. *Energy*, 128: 729–754.

Khandekar, S., Groll, M. 2004. An insight into thermo-hydrodynamic coupling in closed loop pulsating heat pipes. *International Journal of Thermal Sciences*, 43: 13–20.

Khandekar, S., Groll, M., Charoensawan, P., Rittidech, S., Terdtoon, P. 2004. Closed and open loop pulsating heat pipes. In: Proceedings of the 13th International Heat Pipe Conference.

Kim, J., Kim, S. J. 2020. Experimental investigation on working fluid selection in a micro pulsating heat pipe. *Energy Conversion and Management*, 205: 112462.

Ling, L., Zhang, Q., Yu, Y., Liao, S. 2021. A state-of-the-art review on the application of heat pipe system in data centers. *Applied Thermal Engineering*, 199: 117618.

Lu, X., Liu, J., Xu, X. 2016. Contact angle measurements of pure refrigerants. *International Journal of Heat and Mass Transfer*, 102: 877–883.

Ma, H. 2015. Maximum radius of microchannels in an OHP. In: *Oscillating Heat Pipes*, New York: Springer, 147.

Mameli, M., Besagni G., Bansal, P. K., Markides, C. N. 2022. Innovations in pulsating heat pipes: From origins to future perspectives. *Applied Thermal Engineering*, 203: 117921.

Moffat, R. J. 1988. Describing the uncertainties in experimental results. *Experimental Thermal and Fluid Science*, 1: 3–17.

National Institute of Standards and Technology. 2013. mini-REFPROP - Version 10.0. U.S. Department of Commerce. Available at https://trc.nist.gov/refprop/MINIREF/MINIREF.HTM

Nikolayev, V. S. 2021. Physical principles and state-of-the-art of modeling of the pulsating heat pipe: A review. *Applied Thermal Engineering*, 195: 117111.

Pachghare, P. R., Mahalle, A. M. 2013. Effect of pure and binary fluids on closed loop pulsating heat pipe thermal performance. *Procedia Engineering*, 51: 624–629.

Qu, J., Wu, H., Cheng, P. 2012. Start-up, heat transfer and flow characteristics of silicon-based micro pulsating heat pipes. *International Journal of Heat and Mass Transfer*, 55: 6109–6120.

Quan, L., Jia, L. 2009. Experimental study on heat transfer characteristic of plate pulsating heat pipe. In: Proceedings of the ASME 2nd International Conference on Micro/Nanoscale Heat and Mass Transfer, Shanghai, China: 361–366.

Rainieri, S., Bozzoli, F., Pagliarini, G. 2008. Characterization of an uncooled infrared thermographic system suitable for the solution of the 2-D inverse heat conduction problem. *Experimental Thermal and Fluid Science*, 32: 1492–1498.

Rao, Z., Wang, S., Wu, M., Lin, Z., Li, F. 2013. Experimental investigation on thermal management of electric vehicle battery with heat pipe. *Energy Conversion and Management*, 65: 92–97.

Saha, M., Feroz, C. M., Ahmed, F., Mujib, T. 2012. Thermal performance of an open loop closed end pulsating heat pipe. *Heat and Mass Transfer*, 48: 259–265.

Sohel Murshed, S. M., Nieto de Castro, C. A. 2017. A critical review of traditional and emerging techniques and fluids for electronics cooling. *Renewable and Sustainable Energy Reviews*, 78: 821–833.

Taft, B. S., Williams, A. D., Drolen, B. L. 2012. Review of pulsating heat pipe working fluid selection. *Journal of Thermophysics and Heat Transfer*, 26: 651–656.

Vadgama, B., Harris, D. K. 2007. Measurements of the contact angle between R134a and both aluminum and copper surfaces. *Experimental Thermal and Fluid Science*, 31: 979–984.

Yang, H., Khandekar, S., Groll, M. 2008. Operational limit of closed loop pulsating heat pipes. *Applied Thermal Engineering*, 28: 49–59.

Yin, D., Wang, H., Ma, H. B., Ji, Y. L. 2016. Operation limitation of an oscillating heat pipe. *International Journal of Heat and Mass Transfer*, 94: 366–372.

Zhang, D., He, Z., Guan, J., Tang, S., Shen, C. 2022. Heat transfer and flow visualization of pulsating heat pipe with silica nanofluid: An experimental study. *International Journal of Heat and Mass Transfer*, 183: 122100.

Zhang, Y., Faghri, A. 2008. Advances and unsolved issues in pulsating heat pipe. *Heat Transfer Engineering*, 19: 20–44.